IEEE Access
Multidisciplinary | Rapid Review | Open Access Journal

Received November 10, 2019, accepted November 27, 2019, date of publication December 9, 2019,
date of current version December 23, 2019.

Digital Object Identifier 10.1109/ACCESS.2019.2958320

Static Gait Planning Method for Quadruped Robot Walking on Unknown Rough Terrain

SHUAISHUAI ZHANG[1], MING LIU[1,2], YANFANG YIN[1], XUEWEN RONG[2], YIBIN LI[2], AND ZISEN HUA[2]

[1]Department of Electrical Engineering and Information Technology, Shandong University of Science and Technology, Jinan 250031, China
[2]School of Control Science and Engineering, Shandong University, Jinan 250061, China

Corresponding author: Shuaishuai Zhang (zhangshuaisdu@163.com)

This work was supported in part by the National Natural Science Foundation of China under Grant 61703243 and Grant U1613223, in part by the Major Program of Shandong Province Natural Science Foundation under Grant ZR2018ZC0437, and in part by the Major Scientific and Technological Innovation Projects of Shandong Province under Grant 2017CXGC0908.

ABSTRACT To enable quadruped robot to walk through unknown rough terrains without any machine vision system, a continuous static gait planning method is proposed in this paper. A algorithm for on-line terrain complexity evaluation according to touchdown times of swing feet is presented to make quadruped robot obtain the information of terrain without relying on machine vision system. Quadruped robot can obtain enough stability margin during walking process by using the proposed body trajectory planning method, and motion continuity of body can be guaranteed. In order to improve the terrain adaptability of quadruped robot, a tunable parameter is set in the body planning method, and the relationship between value of the tunable parameter and terrain complexity estimation is given to further improve terrain adaptability and energy utilization rate. With the proposed static gait generation method, quadruped robot can autonomous plan its static gait in real-time and travel over unknown rough terrains with enough stability margin. The simulation results show the correctness and effectiveness of the proposed method.

INDEX TERMS Quadruped robot, static gait planning, estimation of terrain complexity, foot swing trajectory.

I. INTRODUCTION

Quadruped robots can walk on rough terrains, even on complex terrain that wheeled and tracked robots cannot cross [1]. In many research fields of quadruped robots, gait planning is one of the most basic and important aspects. A robust gait can help quadruped robot to pass through different types of rough terrain, especially those unstructured and natural terrain with high complexity. Among a variety of quadrupedal gaits, quadruped robots usually choose static gait to improve their walking stability. In the research of static gait, McGhee and Frank first give the mathematical description of the static gait of quadruped robot [2]. After that, many scholars proposed the methods of static gait planning for quadruped robots.

Ma *et al.* [3] proposed a successive gait-transition method for quadruped robot to realize omnidirectional static walking. Hwang and Youm [4] developed a steady crawl gait. The main feature of the suggested algorithm is that it is not based on foothold selection and it can be used for the walking of blind robots on more realistic irregular terrain. Santos and Matos [5] developed a quadruped locomotion controller able to generate omnidirectional locomotion and a path planning controller for heading direction. Chen *et al.* [6] presented translational crawl and path tracking for a quadruped robot named TITAN-VIII, to walk on rough ground. Loc *et al.* [7] presented a study on improving the traversability of a quadruped walking robot in 3D rough terrains. In these methods, terrain information are not taken into account in gait planning of quadruped robot. When quadruped robots use these methods, they are prone to lose stability because of influence of terrain changes.

In order to improve terrain adaptability, quadruped robot must be able to obtain terrain information and adjust its motion mode or gait parameters according to the obtained information. Equipped with machine vision system for quadruped robots is the main way to obtain terrain information. Fankhauser *et al.* [8] presented a motion planner for the

The associate editor coordinating the review of this manuscript and approving it for publication was Okyay Kaynak.

perceptive rough terrain locomotion with quadrupedal robots. The planner finds safe footholds along with collision-free swing-leg motions by leveraging an acquired terrain map. They experimentally validated the proposed approach with the quadrupedal robot ANYmal by autonomously traversing obstacles such steps, inclines, and stairs. Bazeille *et al.* [9] presented a framework for a quadruped robot, which performs goal-oriented navigation on unknown rough terrain by using inertial measurement data and stereo vision. By using accurate a-priori given maps and external robot state sensors, some gait planning methods were presented by different teams for the quadruped robot named Little-Dog travelling over different types of rough terrains [10]–[16], and the feasibility and effectiveness of these methods in practical applications were analyzed through the experimental results. Havoutis *et al.* [17] presented a framework that utilizes on-board perception to adapt a large quadruped's behaviour according to the situation at hand. The proposed framework can switch between a dynamic trot and a stable crawl gait. Winkler *et al.* [18] presented a framework for dynamic quadrupedal locomotion over challenging. They built a model of the environment on-line and on-board using an efficient occupancy grid representation for a hydraulic quadruped on challenging terrain. Chilian and Hirschmüller [19] developed a navigation algorithm for mobile robots in unknown rough terrain. The algorithm is solely based on stereo images and suitable for wheeled and legged robots. Based on stereo vision, Shao *et al.* [20] proposed a locomotion control system for a quadruped robot that is able to perform adaptive locomotion in unknown environments cluttered with many obstacles. Wermelinger *et al.* [21] presented a framework for planning safe and efficient paths for a legged robot in rough and unstructured terrain. Typical terrain characteristics were computed such as slope, roughness, and steps to build a traversability map. By using these methods, although quadruped robot can accurately obtain terrain information, it needs to equip the robot with complex machine vision systems, and the computational complexity of image information processing is large.

To overcome these shortcomings, this paper presents a continuous static gait generation method for quadruped robots based on on-line terrain complexity estimation. Using the terrain complexity estimation method proposed in this paper, quadruped robot can estimate the complexity of terrain in real time only according to touchdown times of swing feet without relying on machine vision system. According to support pattern of quadruped robot, the body trajectory planning method is given. The proposed method can not only effectively help quadruped robot increase its stability margin, but also ensure that the speed and acceleration of body motion are all continuous. According to the proposed relationship between the estimated terrain complexity and the tunable parameter in body trajectory planning method, quadruped robot can determine independently the value of tunable parameter according to terrain complexity estimation, thus improving terrain adaptability and energy utilization rate of quadruped robot.

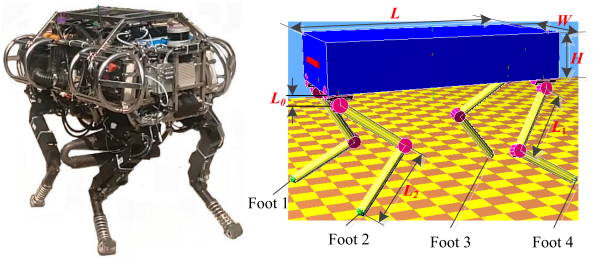

(a)Prototype of the hydraulic actuated quadruped robot

(b)Simulation model of the hydraulic actuated quadruped robot

FIGURE 1. The prototype and simulation model of the hydraulic actuated quadruped robot.

TABLE 1. The major specifications of the hydraulic actuated robot model.

Body	Mass	90Kg	
	Dimensions	Length(L_B)	0.7m
		Width(W_B)	0.35m
		Heigh(H_B)	0.2m
Leg	Mass	10Kg	
	Dimensions	L_0	0.05m
		L_1	0.3m
		L_2	0.3m

The simulation results verify the correctness and effectiveness of the proposed method.

II. THE MODEL AND THE COORDINATE FRAMES OF THE QUADRUPED ROBOT

The evaluation of our approach is done on the simulation model of a hydraulic actuated quadruped robot. Fig.1 provides the prototype of the hydraulic actuated quadruped robot and its simulation model established in the software Webots.

The major specifications of the hydraulic actuated robot model are listed in table 1, and the coordinate frames related to the gait generation method proposed in this paper are shown in the Fig.2. The four red crossed in the Fig.2 represent the projection of the four support points correspond to the four support feet projected on the horizontal plane, respectively.

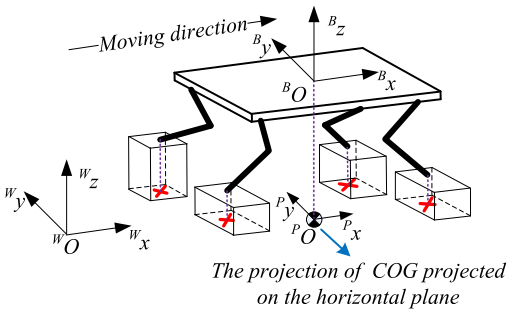

FIGURE 2. The coordinate frames related to the gait planning method proposed in this paper.

The body coordinate frame $\{^BO\}$ is defined with its origin at the *COG*(Center of Gravity) of the body of robot, and the ^Bx axis is pointing forward. The ^Bz axis of the coordinate frame $\{^BO\}$ is pointing upward, and the direction of the ^By axis is determined by the right hand rule. The origin of the coordinate frame $\{^PO\}$ is located at the vertical projection of the *COG* (projected on the horizontal ground) with the ^Px axis parallel with the forward direction. The ^Pz axis of the coordinate frame $\{^PO\}$ is pointing to the opposite direction of the gravity and the ^Py axis of the coordinate frame $\{^PO\}$ parallel with the ^Py axis of the $\{^BO\}$. The world coordinate frame $\{^WO\}$ with its origin fixed on the ground is the major reference of the overall system.

III. THE FOOT SWING SEQUENCE OF THE PROPOSED STATIC GAIT

The use of an appropriate foot swing sequence is helpful for improving walking stability of quadruped robot. There are six different foot swing sequences of non-singular quadrupedal static gaits proved by McGhee and Frank [2]. Among these six foot swing sequences, there is only one foot swing sequence, 4-2-3-1(the foot no. is shown in Fig.1), can be used to ensure stability of quadruped robot with the COG move forward at all times [22]. Therefore, this foot swing sequence is chosen for quadruped robot motion planning in this paper.

Although the support triangles corresponding to different swing feet are different, there is a triangle-shaped intersection of two subsequent support triangles of hind and front swing feet on the same side of robot's body. This intersection is called a "double support triangle" (DST) [10], [12] and is often used in body trajectory planning for static walk of quadruped robot. Taking the support pattern of the robot shown in Fig.3 as an example, the dotted and dashed triangle represent the support triangle of a hind foot and a front foot respectively, and the red sold triangle is a DST.

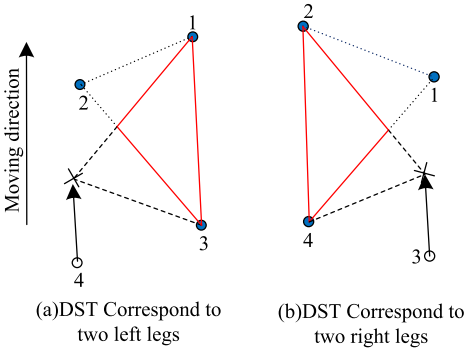

FIGURE 3. A diagram of DST.

Given the minimum static stability margin (S_{min}) requirement, the shadow areas shown in Fig. 4 are the stable areas for the swing movements of the corresponding two ipsilateral feet. When projection of COG located in these area, the front foot can be lifted up stably just after the hind foot on the same side of body touches the ground. From the Fig.4, it can

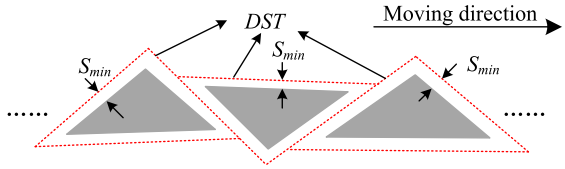

FIGURE 4. The stable regions during moving of quadruped robot.

be seen that the stable areas respectively correspond to the swing movements of the left two feet and the right two feet are disjoint because of the presence of the S_{min}. Whenever quadruped robot completes the swing movements of the two feet on the same side in turn, a body sway phase (*BSP*) is necessary to move the COG from the current DST to the following DST before the hind feet on the other side swing forward to guarantee the stability of quadruped robot no less than the value of S_{min} in the whole walking process of quadruped robot.

In this paper, the whole walking process of quadruped robot is divided into N (N>0) gait cycles, and a single gait cycle includes two *BSPs* and two foot swing phases(*FSPs*). In *FSP*, two legs on the same side of robot's body complete their swing movement in turn according to the foot swing sequence.

IV. THE COG TRAJECTORY PLANNING METHOD BASED ON ON-LINE TERRAIN COMPLEXITY ESTIMATION

A method of body trajectory planning method based on quintic equation which can help quadruped robot guarantees its stability and continuity of motion is given in this paper. A tunable parameter of body trajectory planning can automatically be determined according to the evaluation value of terrain complexity, and the terrain adaptability of quadruped robot can be improved.

A. THE METHOD OF ON-LINE TERRAIN COMPLEXITY ESTIMATION

In the proposed gait planning method, rectangular trajectory of swing foot is used to guide swing foot move to the target foothold. The rectangular trajectory of swing foot can be divided into three parts: the vertical rising part, the horizontal movement part and the vertical dropping part, as shown in Fig.5.

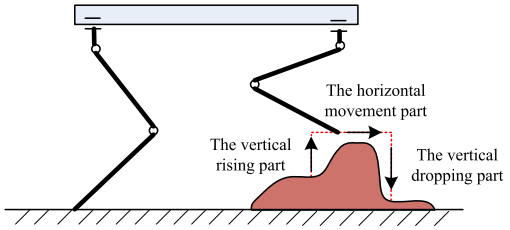

FIGURE 5. The diagram of foot trajectory generated in this paper.

Let ^mt_i ($i \in [1, 2, 3, 4]$) be the elapsed time from the start to the end of the third part of swing movement of the foot i

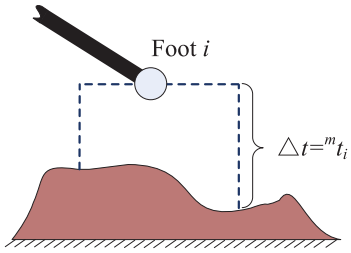

FIGURE 6. The touchdown time ${}^{m}t_i$ of swing foot i.

in the m-th gait cycle, as shown in Fig.6. This paper presents an on-line terrain complexity estimation method by using the ${}^{m}t_i$ to estimate the complexity of the terrain which robot travel over in the m-th gait cycle in real time.

In the m-th gait cycle, the standard deviation of ${}^{m}t_i$ can be obtained by (1).

$$\begin{cases} \bar{t} = \dfrac{\sum_{i=1}^{4} {}^{m}t_i}{4} \\ {}^{t}\sigma_m = \sqrt{\dfrac{\sum_{i=1}^{4} \left({}^{m}t_i - \bar{t}\right)^2}{4}} \end{cases} \tag{1}$$

In this paper, second-order exponential smoothing model is applied to the prediction of estimation terrain complexity in the $(m+1)$-th gait cycle, and use the estimated result to set the value of tunable parameter in the proposed body trajectory generation of quadruped robot.

In the proposed method, the second-order smoothing value $s_m^{(2)}$ is calculated based in part on a weighted average (using the weighting factor α) of the first-order smoothing value $s_m^{(1)}$ of the estimation terrain complexity in current gait cycle and the previous second-order smoothing value $s_{m-1}^{(2)}$ associated with estimation terrain complexity in the previous gait cycle, as shown in (2).

$$\begin{cases} s_m^{(1)} = \alpha \cdot \phi_m + (1-\alpha) \cdot s_{m-1}^{(1)} \\ s_m^{(2)} = \alpha \cdot s_m^{(1)} + (1-\alpha) \cdot s_{m-1}^{(2)} \end{cases} \tag{2}$$

where $\phi_m = \dfrac{\sum_{p=m-q+1}^{m} {}^{t}\sigma_p}{q}$, $q \geq 1$

Then the prediction of estimation terrain complexity in the $(m+1)$-th gait cycle can be obtained by (3).

$$\widehat{R}_{m+1} = \lambda_m + \beta_m \tag{3}$$

where $\begin{cases} \lambda_m = 2S_m^{(1)} - S_m^{(2)} \\ \beta_m = \frac{\alpha}{1-\alpha}\left(S_m^{(1)} - S_m^{(2)}\right) \end{cases}$

B. THE BODY TRAJECTORY PLANNING METHOD

In the gait planning method proposed in this paper, the body of quadruped robot completes a body sway movement to ensure it can complete the movement of swing foot stably in the *BSP*, and the body of quadruped robot move uniformly in a straight line in *FSP*.

Let ${}^{B}P$ $({}^{BSP}x_E, {}^{BSP}y_E)$ be the desired position of the projection of the COG and its coordinate which is repressed in the coordinate system $\{{}^{P}O\}$ when the robot finishes *BSP*. Similarly, let ${}^{F}P$ $({}^{FSP}x_E, {}^{FSP}y_E)$ be the desired position of the projection of the COG at the end of *FSP* and its coordinate which is repressed in the coordinate system $\{{}^{P}O\}$. The positions of the ${}^{B}P$ and ${}^{F}P$ should be respectively determined to obtain body trajectory.

In the body trajectory planning, the coordinate system $\{{}^{P}O\}$, as shown in the Fig.3, is the main reference coordinate framework. A coordinate frame system $\{{}^{B_0}O\}$ is defined with its origin coincident with origin of $\{{}^{B}O\}$ to determine the projections of footholds of four support feet in *BSP* in the coordinate $\{{}^{P}O\}$, and further generate body trajectory. The three axes of the $\{{}^{B_0}O\}$ parallel to the three axes of the world coordinate frame system $\{{}^{W}O\}$ respectively.

Let ${}^{B}F_s({}^{B}y_s, {}^{B}z_s)$ be the coordinate values of the foothold of the foot s $(s \in [1,2,3,4])$ which is expressed in the coordinate frame $\{{}^{B}O\}$, and let θ and β be the pitching angle and the rolling angle of body of quadruped robot respectively. The value of the θ and β can be obtained from the IMU (Inertial measurement unit) which is mounted on the body of robot in real-time. Then, the foothold of the $s-th$ foot which is expressed in the coordinate system $\{{}^{B_0}O\}$ can be obtained as follow:

$$\begin{aligned} {}^{B_0}P_s &= \begin{bmatrix} {}^{B_0}x_s \\ {}^{B_0}y_s \\ {}^{B_0}z_s \\ 1 \end{bmatrix} \\ &= \begin{bmatrix} c\theta & s\theta s\beta & c\beta s\theta & 0 \\ 0 & c\beta & -s\beta & 0 \\ -s\theta & c\theta s\beta & c\theta c\beta & 0 \\ 0 & 0 & 0 & 1 \end{bmatrix} \cdot \begin{bmatrix} {}^{B}x_s \\ {}^{B}y_s \\ {}^{B}z_s \\ 1 \end{bmatrix} \\ &= \begin{bmatrix} {}^{B}x_s \cdot c\theta + {}^{B}z_s \cdot c\beta \cdot s\theta + {}^{B}y_s \cdot s\theta \cdot s\beta \\ {}^{B}y_s \cdot c\beta - {}^{B}z_s \cdot s\beta \\ {}^{B}z_s \cdot c\theta \cdot c\beta + {}^{B}x_s \cdot s\theta + {}^{B}y_s \cdot c\theta \cdot s\beta \\ 1 \end{bmatrix} \end{aligned} \tag{4}$$

where $\begin{cases} s\theta = \sin\theta \\ c\theta = \cos\theta \\ s\beta = \sin\beta \\ c\beta = \cos\beta \end{cases}$

Because the ${}^{B_0}x$ and ${}^{B_0}y$ are parallel to ${}^{P}x$ and ${}^{P}y$ respectively, the coordinate of the foothold of foot s which is expressed in the coordinate system $\{{}^{P}O\}$ can be obtained in (5) according to (4).

$$\begin{cases} {}^{p}x_s = {}^{B}x_s \cdot c\theta + {}^{B}z_s \cdot c\beta \cdot s\theta + {}^{B}y_s \cdot s\theta \cdot s\beta \\ {}^{p}y_s = {}^{B}y_s \cdot c\beta - {}^{B}z_s \cdot s\beta \end{cases} \tag{5}$$

In order to facilitate description of the proposed body trajectory planning method, the labels are assigned for the four footholds between support feet and terrain in the coordinate system $\{{}^{P}O\}$ when robot is in *BSP*. As shown in Fig.7, let $P_{NSF}({}^{P}x_{NSF}, {}^{P}y_{NSF})$ and $P_{DF}({}^{P}x_{DF}, {}^{P}y_{DF})$ be projection of the foot-end of the next swing foot (*NSF*) according to the

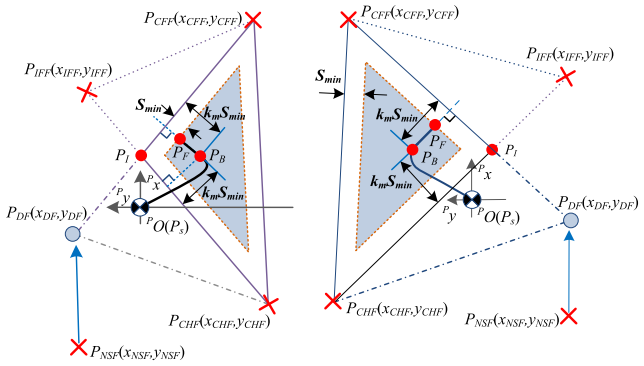

FIGURE 7. The related parameters in the COG trajectory generation.

foot swing sequence and projection of the desired foothold of *NSF*, and let $P_{IFF}({}^{P}x_{IFF}, {}^{P}y_{IFF})$ be the projection point of the foot-end of the foot on the same side of body with *NSF*. Meanwhile, let $P_{CFF}({}^{P}x_{CFF}, {}^{P}y_{CFF})$ and $P_{CHF}({}^{P}x_{CHF}, {}^{P}y_{CHF})$ respectively be the projection points of the foot-ends correspond to front foot and hind foot of the remaining two feet.

Let L_{DF-CFF} be the line joining a pair of points P_{DF} and P_{CFF}, and let $L_{IFF-CHF}$ be the line joining a pair of points P_{IFF} and P_{CHF}. According to the coordinate value of the points P_{DF}, P_{CFF}, P_{CHF} and P_{IFF}, the equations of the L_{DF-CFF} and $L_{IFF-CHF}$ can be obtained as follow:

$$\begin{cases} f_{DF-CFF}(x) = k_{DF-CFF} \cdot x + b_{DF-CFF} \\ = \dfrac{{}^{P}y_{DF} - {}^{P}y_{CFF}}{{}^{P}x_{DF} - {}^{P}x_{CFF}} \cdot x + {}^{P}y_{DF} - \dfrac{{}^{P}y_{DF} - {}^{P}y_{CFF}}{{}^{P}x_{DF} - {}^{P}x_{CFF}} \cdot {}^{P}x_{DF} \\ f_{IFF-CHF}(x) = k_{IFF-CHF} \cdot x + b_{IFF-CHF} \\ = \dfrac{{}^{P}y_{IFF} - {}^{P}y_{CHF}}{{}^{P}x_{IFF} - {}^{P}x_{CHF}} \cdot x + y_{IFF} - \dfrac{{}^{P}y_{IFF} - {}^{P}y_{CHF}}{{}^{P}x_{IFF} - {}^{P}x_{CHF}} \cdot x_{IFF} \end{cases} \tag{6}$$

According to (6), the coordinate value of intersection point between the L_{DF-CFF} and the $L_{IFF-CHF}$, labeled $P_I({}^{P}x_I, {}^{P}y_I)$, can be obtained by (7).

$$\begin{cases} {}^{P}x_I = \dfrac{b_{DF-CFF} - b_{IFF-CHF}}{k_{IFF-CHF} - k_{DF-CFF}} \\ {}^{P}y_I = k_{IFF-CHF} \cdot {}^{P}x_I + b_{IFF-CHF} \end{cases} \tag{7}$$

The triangle $\triangle P_I P_{CFF} P_{CHF}$ is a DST corresponding to *FSF* and *IFF*, as shown in Fig.7. The inner point of the $\triangle P_I P_{CFF} P_{CHF}$, labeled P_C $({}^{P}x_C, {}^{P}y_C)$, can be obtained from the coordinates of the vertexes of the double-supported triangle, as shown in (8).

$$\begin{bmatrix} {}^{P}x_C \\ {}^{P}y_C \end{bmatrix} = \begin{bmatrix} \dfrac{{}^{P}x_I \cdot \|\alpha\|_2 + {}^{P}x_{CFF} \cdot \|\beta\|_2 + {}^{P}x_{CHF} \cdot \|\gamma\|_2}{\|\alpha\|_2 + \|\beta\|_2 + \|\gamma\|_2} \\ \dfrac{{}^{P}y_I \cdot \|\alpha\|_2 + {}^{P}y_{CHF} \cdot \|\beta\|_2 + {}^{P}y_{CHF} \cdot \|\gamma\|_2}{\|\alpha\|_2 + \|\beta\|_2 + \|\gamma\|_2} \end{bmatrix} \tag{8}$$

where

$$\begin{cases} V_a = \begin{bmatrix} x_I & y_I \end{bmatrix}^T \\ V_b = \begin{bmatrix} {}^{P}x_{CFF} & {}^{P}y_{CFF} \end{bmatrix}^T \\ V_c = \begin{bmatrix} {}^{P}x_{CHF} & {}^{P}y_{CHF} \end{bmatrix}^T \\ \alpha = V_c - V_b, \beta = V_a - V_c, \gamma = V_b - V_a \end{cases}$$

Let ${}^{m}k$ be the tunable parameter in body trajectory planning, and ${}^{B}P$ should be the point which satisfy (9) in $\triangle P_I P_{CFF} P_{CHF}$.

$$\begin{cases} {}^{DF-CFF}D_{\perp}\left({}^{BSP}x_E\, {}^{BSP}y_E\right) = {}^{m}k \cdot S_{\min} \\ {}^{IFF-CHF}D_{\perp}\left({}^{BSP}x_E\, {}^{BSP}y_E\right) = {}^{m}k \cdot S_{\min} \\ {}^{B}P \in \triangle P_I P_{CFF} P_{CHF} \end{cases} \tag{9}$$

where ${}^{DF-CFF}D_{\perp}$ and ${}^{IFF-CHF}D_{\perp}$ respectively be the vertical distance from point ${}^{B}P$ to the line L_{DF-CFF} and $L_{IFF-CHF}$.

According to (9), the coordinates of point ${}^{B}P$ in coordinate system $\{{}^{P}O\}$ can be obtained, as shown in (10).

$$\begin{cases} {}^{BSP}x_E = {}^{P}x_I + {}^{m}k \cdot sign\left({}^{P}y_C - {}^{P}y_I\right) \cdot \frac{S_{\min}}{\sin\alpha} \cdot \cos\beta \\ {}^{BSP}y_E = k_{IC} \cdot {}^{BSP}x_E + b_{IC} \end{cases} \tag{10}$$

where

$$\begin{cases} \alpha = \arccos \dfrac{m \cdot n}{\|m\|_2 \cdot \|n\|_2} \\ m = \left({}^{P}x_{CFF} - {}^{P}x_I, {}^{P}y_{CFF} - {}^{P}y_I\right) \\ n = \left({}^{P}x_{CHF} - {}^{P}x_I, {}^{P}y_{CHF} - {}^{P}y_I\right) \\ \beta = \arctan \dfrac{{}^{P}y_P - {}^{P}y_I}{{}^{P}x_P - {}^{P}x_I} \\ k_{IC} = \dfrac{{}^{P}y_I - {}^{P}y_C}{{}^{P}x_I - {}^{P}x_C} \\ b_{IC} = {}^{P}y_I - k_{IC} \cdot {}^{P}x_I \end{cases}$$

Let ${}^{DF-CFF}L_{\perp}$ be the the line that crosses ${}^{BSP}P_E$ and perpendicular to L_{DF-CFF}, and ${}^{F}P({}^{F}x, {}^{F}y)$ is the point located on line ${}^{DF-CFF}L_{\perp}$ which satisfy (11).

$$\begin{cases} {}^{DF-CFF}D_{\perp}\left({}^{FSP}x_E\, {}^{FSP}y_E\right) = S_{\min} \\ {}^{FSP}y_E = {}^{DF-NF}k_{\perp} \cdot {}^{FSP}x_E + {}^{DF-NF}b_{\perp} \\ {}^{F}P \in \Delta_{DST} \end{cases} \tag{11}$$

where ${}^{DF-CFF}D_{\perp}\left({}^{FSP}x_E\, {}^{FSP}y_E\right)$ represents vertical distance from point ${}^{F}P$ to line L_{DF-CFF}.

According to (11), the coordinates of the point ${}^{F}P$ in the coordinate system $\{{}^{P}O\}$ can be obtained, as shown in (12).

$$\begin{cases} {}^{FSP}x_E = \bar{x} - sign\left(\bar{x} - {}^{BSP}x_E\right) \cdot \sqrt{\Delta_x} \\ {}^{FSP}y_E = \bar{y} - sign\left(\bar{y} - {}^{BSP}y_E\right) \cdot \sqrt{\Delta_y} \end{cases} \tag{12}$$

where

$$\begin{cases} \Delta_x = \dfrac{(k_{CFF-DF} \cdot S_{\min})^2}{{k_{CFF-DF}}^2 + 1} \\ \Delta_y = -\dfrac{\sqrt{\Delta_x}}{k_{CFF-DF}} \\ \bar{x} = \dfrac{{}^{BSP}x_E + k_{CFF-DF} \cdot {}^{BSP}y_E - k_{CFF-DF} \cdot b_{CFF-DF}}{{k_{CFF-DF}}^2 + 1} \\ \bar{y} = \dfrac{k_{CFF-DF} \cdot {}^{BSP}x_E + {k_{CFF-DF}}^2 \cdot {}^{BSP}y_E + b_{CFF-DF}}{{k_{CFF-DF}}^2 + 1} \end{cases}$$

In order to ensure the motion continuity of robot's body in *BSP*, according to the determined coordinates of point ${}^{B}P$ and ${}^{F}P$, a method of generating the body trajectory based on quintic equation is proposed. In following part, the equations of body trajectory in *BSP* and *FSP* are given respectively.

1) EQUATION OF BODY TRAJECTORY IN *BSP*

The equation of body trajectory based on quintic equation in *BSP* is shown in (13).

$$\begin{cases} {}^{BSP}x_{COG}(t) = {}^{x}p_5 \cdot t^5 + {}^{x}p_4 \cdot t^4 + {}^{x}p_3 \cdot t^3 \\ + {}^{x}p_2 \cdot t^2 + {}^{x}p_1 \cdot t + {}^{x}p_0 \\ = {}^{x}p^T \cdot \phi \\ {}^{BSP}y_{COG}(t) = {}^{y}p_5 \cdot t^5 + {}^{y}p_4 \cdot t^4 + {}^{y}p_3 \cdot t^3 \\ + {}^{y}p_2 \cdot t^2 + {}^{y}p_1 \cdot t + {}^{y}p_0 \\ = {}^{y}p^T \cdot \phi \end{cases} \tag{13}$$

where

$$\begin{cases} {}^{x}p^T = \begin{bmatrix} {}^{x}p_5 & {}^{x}p_4 & {}^{x}p_3 & {}^{x}p_2 & {}^{x}p_1 & {}^{x}p_0 \end{bmatrix} \\ {}^{y}p^T = \begin{bmatrix} {}^{y}p_5 & {}^{y}p_4 & {}^{y}p_3 & {}^{y}p_2 & {}^{y}p_1 & {}^{y}p_0 \end{bmatrix} \\ \phi^T = \begin{bmatrix} t^5 & t^4 & t^3 & t^2 & t & 1 \end{bmatrix} \\ t \in [0, T_{BSP}], \end{cases}$$

T_{BSP} represents the planned time for quadruped robot to complete *BSP*.

In *BSP*, the origin of coordinate system $\{{}^{P}O\}$ and the point ${}^{B}P$ respectively be the starting point and the end point of the body movement, that is, the position condition of the body trajectory meets (14).

$$\begin{cases} {}^{BSP}f_x(t)\,|_{t=0} = {}^{BSP}f_y(t)\,|_{t=0} = 0 \\ {}^{BSP}f_x(t)\,\big|_{t=T_{BSP}} = {}^{BSP}x_E \\ {}^{BSP}f_y(t)\,\big|_{t=T_{BSP}} = {}^{BSP}y_E \end{cases} \tag{14}$$

The body of robot only moves in a uniform straight line in *FSF*, and there are *FSFs* just before and after *BSF* of robot. Therefore, the boundary conditions of the velocity and acceleration of body trajectory in the direction of ${}^{P}y$ are shown in (15).

$$\begin{cases} \ddot{{}^{BSP}f_x}(t)\,|_{t=0} = \ddot{{}^{BSP}f_x}(t)\,\big|_{t=T_{BSP}} = 0 \\ \ddot{{}^{BSP}f_y}(t)\,|_{t=0} = \ddot{{}^{BSP}f_y}(t)\,\big|_{t=T_{BSP}} = 0 \\ \dot{{}^{BSP}f_x}(t)\,\big|_{t=0} = {}^{COG}v_{x0} \\ \dot{{}^{BSP}f_y}(t)\,\big|_{t=0} = {}^{COG}v_{y0} \\ \dot{{}^{BSP}f_x}(t)\,\big|_{t=T_{BSP}} = {}^{COG}V_x = \dfrac{{}^{FSP}x_E - {}^{BSP}x_E}{T_{FSP}} \\ \dot{{}^{BSP}f_y}(t)\,\big|_{t=T_{BSP}} = {}^{COG}V_y = \dfrac{{}^{FSP}y_E - {}^{BSP}y_E}{T_{FSP}} \end{cases} \tag{15}$$

where ${}^{COG}v_{x0}$ and ${}^{COG}v_{y0}$ are the initial velocity of body in the direction of ${}^{P}x$ and ${}^{P}y$ at the initial moment of *BSP*.

Then, according to the boundary conditions of the body trajectory given in (14) and (15), the coefficients of the equation ${}^{BSP}f_y(t)$(as shown in (13)) can be obtained, as shown in (16).

$$\begin{cases} {}^{x}p = p\left(D_x, M_x, {}^{COG}v_{x0}\right) \\ {}^{y}p = p\left(D_y, M_y, {}^{COG}v_{y0}\right) \end{cases} \tag{16}$$

where

$$\begin{cases} M_x = {}^{BSP}x_E \\ M_y = {}^{BSP}y_E \\ D_x = {}^{FSP}x_E - {}^{BSP}x_E \\ D_y = {}^{FSP}y_E - {}^{BSP}y_E \\ p\,(L, M, v_0) \\ = \begin{bmatrix} -\dfrac{3 \cdot (L \cdot T_{BSP} - 2M \cdot T_{FSP} + T_{BSP} \cdot T_{FSP} \cdot v_0)}{{T_{BSP}}^5 \cdot T_{FSP}} \\ \dfrac{7^F L \cdot T_{BSP} - 15M \cdot T_2 + 8T_{BSP} \cdot T_{FSP} \cdot v_0}{{T_{BSP}}^4 \cdot T_{FSP}} \\ -\dfrac{2 \cdot \left(2^F L \cdot T_{BSP} - 5M \cdot T_2 + 3T_{BSP} \cdot T_{FSP} \cdot v_0\right)}{{T_{BSP}}^3 \cdot T_{FSP}} \\ 0 \\ v_0 \\ 0 \end{bmatrix} \end{cases}$$

Finally, by substituting the coefficients in (16) into (13), the trajectory equation of body in *BSP* can be obtained.

2) EQUATION OF BODY TRAJECTORY IN *FSP*

In *FSP*, the body of the robot only moves in a uniform straight line along the forward direction. The ${}^{F}P$ and ${}^{B}P$ respectively be the starting point and the end point of body movement in *FSP*, and thus the position condition of the body trajectory in *FSP* meets (17).

$$\begin{cases} {}^{BSP}f_x(t)\,\big|_{t=T_{BSP}+T_{FSP}} = {}^{FSP}x_E \\ {}^{BSP}f_y(t)\,\big|_{t=T_{BSP}+T_{FSP}} = {}^{FSP}y_E \end{cases} \tag{17}$$

According to (17), the equation of body trajectory along the ${}^{P}x$ direction of the robot in *FSP* can be obtained, as shown

in (18).

$$\begin{cases} {}^{FSP}x_{COG}(t) = {}^{BSP}x_E + {}^{COG}V_x \cdot t \\ = {}^{BSP}x_E + \dfrac{{}^{FSP}x_E - {}^{BSP}x_E}{T_{FSP}} \cdot (t - T_{BSP}) \\ {}^{FSP}x_{COG}(t) = {}^{BSP}y_E + {}^{COG}V_y \cdot t \\ = {}^{BSP}y_E + \dfrac{{}^{FSP}y_E - {}^{BSP}y_E}{T_{FSP}} \cdot (t - T_{BSP}) \end{cases} \tag{18}$$

where $t \in [T_{BSP}, T_{BSP} + T_{FSP}]$, T_{FSP} represents the planning time for the robot to complete *FSP*.

C. METHOD FOR DETERMINING TUNABLE PARAMETER IN BODY TRAJECTORY PLANNING

Using the body trajectory planning method given in this paper, quadruped robot can increase its stability margin through the movement in the lateral direction relative to the moving direction during walking. However, the movement of body in the lateral direction increases energy consumption of robot. Therefore, quadruped robot needs to adjust its gait parameters according to the complexity of terrain, and reasonably determine movement distance in the lateral direction to improve the energy utilization rate of robot under the premise of walking stability.

According to (10), in the $m-th$ gait cycle, the change of value of tunable parameter ${}^{m}k$ in body trajectory planning directly affects the position ${}^{B}P$ of body movement in *BSP*, which in turn affects the generation of body trajectory of quadruped robot.

The movement distance of body in the lateral direction relative to moving direction of robot increase with the value of ${}^{m}k$. Therefore, under the premise of satisfying stability constraint of robot, robot should be able to adjust the value of ${}^{m}k$ independently according to estimation of terrain complexity.

In order to ensure walking stability of robot, after the body movement in *BSP*, robot must satisfy the stability constraint. Therefore, the value of ${}^{m}k$ should be greater or equal to 1 to guarantee the stability margin of robot no less than S_{min} in FSP.

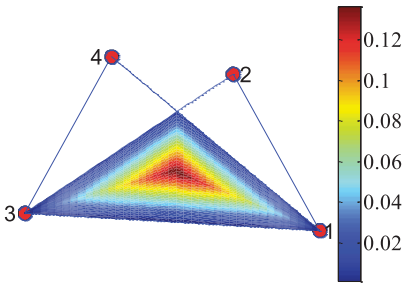

FIGURE 8. The distribution of the stability margin within DST.

Fig.8 shows an example of the distribution of stability margin in DST when robot is in *BSP*. As can be seen from the figure, when the projection of COG is coincide with the inner center of DST, quadruped robot can obtain a greater stability margin. Therefore, in order to ensure the stability of robot during the swing foot movement, the inner point of the DST is desired to be the target point of the body movement in *BSP*. The maximum allowable value ${}^{m}k$, ${}^{m}k_{max}$, can be obtained by (19).

$${}^{m}k_{\max} = \frac{{}^{m}D_{IC} \cdot \sin {}^{m}\gamma}{S_{\min}} \tag{19}$$

where

$$\begin{cases} {}^{m}\gamma = \arccos \dfrac{\vec{p} \cdot \vec{q}}{\left\|\vec{p}\right\|_2 \cdot \left\|\vec{q}\right\|_2} \\ \vec{p} = \left({}^{P}x_C - {}^{P}x_I, {}^{P}y_C - {}^{P}y_I\right) \\ \vec{q} = \left({}^{P}x_{CFF} - {}^{P}x_I, {}^{P}y_{CFF} - {}^{P}y_I\right) \\ {}^{m}D_{IC} = \left\|\vec{p}\right\|_2 \end{cases}$$

According to the estimated terrain complexity in the $(m+1)-th$ gait periods, the calculation method of the coefficient ${}^{m+1}k$ in body trajectory planning is given, as shown in (20).

$$\begin{aligned} {}^{m+1}k &= f_k\left(\widehat{R}_{m+1}\right) \\ &= 1 + \frac{({}^{m}k_{\max} - 1) \cdot \left(\hat{R}_{m+1} - R_{\min}\right)}{(R_{\max} - R_{\min})} \end{aligned} \tag{20}$$

Based on the description in this section, the calculation method of the tunable parameter ${}^{m+1}k$ in body trajectory planning method in the $(m+1)-th$ gait cycle is given in Algorithm 1.

Algorithm 1 The Calculation Method of ${}^{m+1}k$

Input: ${}^{m}t_1$, ${}^{m}t_2$, ${}^{m}t_3$, ${}^{m}t_4$ and q
Output: ${}^{m+1}k$

```
sum ← 0;
R[m] ← ^mσ_t(^m t_i)
while m ≥ 1 do
    if m < q then
        ^{m+1}k ← 1;
    end
    else if m ≥ q then
        for j = 1; j ≤ s; j++ do
            sum ← sum + R[m − j]
        end
        φ_m ← sum/q
    end
    Calculate the prediction of estimation terrain
    complexity in the (m + 1)-th gait cycle R̂_{m+1}
    ^{m+1}k ← f_k(R̂_{m+1})
end
return ^{m+1}k;
```

V. DYNAMICS SIMULATION WITH WEBOTS AND PERFORMANCE ANALYSIS

Fig.9 shows an example test rough terrain established in the simulation software Webots. The simulation is completed by using a computer with Intel i7 3.5GHz processor.

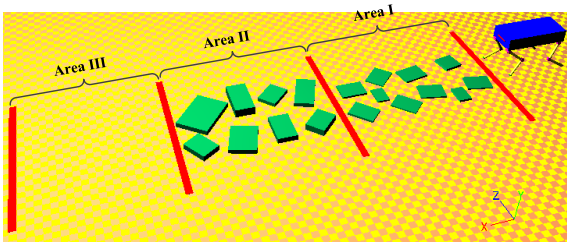

FIGURE 9. An example test rough terrain established in the simulation software Webots.

In the test terrain, Area III a straight and flat road without any obstacles. Obstacles of different sizes and heights are scattered randomly in Area I and Area II, and the average height of the obstacles in Area I is less than that in Area II. The height value of the highest and the lowest obstacle in Area I respectively be 105mm and 20mm, and the mean of all the obstacles is 88mm. Meanwhile, in Area II, the height value of the highest and the lowest obstacle respectively be 215mm and 170 mm, and the mean of all the obstacles is 187mm. Therefore, the complexity of Area I is higher than Area III but lower than Area II.

Because robot had no help of vision system or prior information of the test terrain, the test terrain shown in Fig.9 is unknown and uncertain for the quadruped robot. Fig.10 shows a set of snap-shots when the robot was walking on the rough terrain. According to the static gait planning method proposed in this paper, the robot can plan its motion in real time to pass through the complex terrain stably and autonomously.

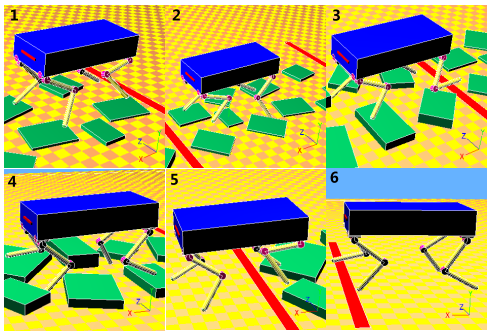

FIGURE 10. Sequence of snapshots of the movement process of the quadruped robot.

According to the touchdown times of swing feet in the walking process of robot, as shown in Fig.11, the terrain complexity estimation $\hat{R}_m$ is given in Fig.12.

The value of estimation of terrain complexity of Area I are higher than Area III but lower than Area II based on the change curve of $\hat{R}_m$ shown in the Fig.12. Therefore, the quadruped robot can estimate the complexity of the terrain in real time, and the result of the terrain complexity estimation is consistent with the actual terrain information. In this way, the quadruped robot effectively realizes the real-time and

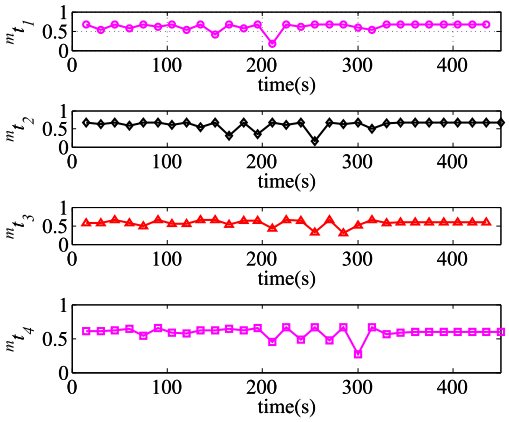

FIGURE 11. The touchdown times of the swing feet during moving of robot.

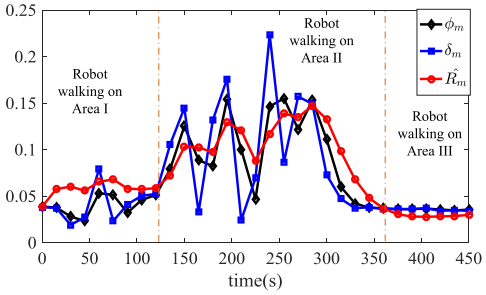

FIGURE 12. Terrain estimation result of robot in walking ($\alpha = 0.3$).

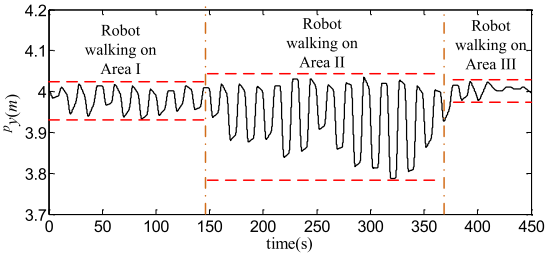

FIGURE 13. The position variation curve of COG along the ^{P}y-axis direction.

accurate estimation of terrain complexity without relying on visual system by using the proposed terrain complexity estimation method.

Fig.14 shows the position variation curve of COG along the ^{P}y-axis direction in the walking process of the robot. From Fig.14, it can be seen that the movement distance of body along the lateral direction change with the estimation of terrain complexity. The adaptability of robot to rough terrain with different complexity can be improved in this way.

The stability margin of the robot during walking is no less than the value of the S_{min} (the value of S_{min} is set to be $50mm$ in the simulation experiment) as shown in the Fig.14. That is, the stability of the robot was effectively guaranteed during the whole walking.

Fig.15 and Fig.16 respectively illustrate the velocity and acceleration variations of the body of robot with respect to

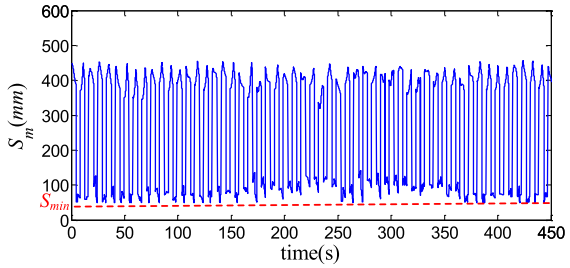

FIGURE 14. The position variation curve of COG along the ^{P}y-axis direction.

world frame $\{^{W}O\}$ when the quadruped robot walking on the test rough terrain shown in Fig.9. It can be concluded that, during the walking processes, the velocity and acceleration variations of the body with respect to world frame $\{^{W}O\}$ are all continuous. In this way, the body of quadruped robot moves in a twice differentially way. So the robot can avoid any form of jerkiness which can lead to foot slipping and instability of the robot by using free gait generation method proposed in this paper.

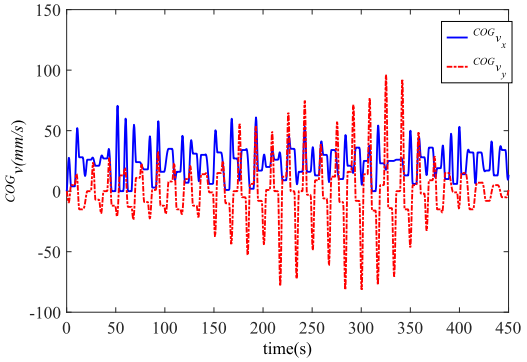

FIGURE 15. The acceleration variation curve of COG with respect to $\{^{W}O\}$.

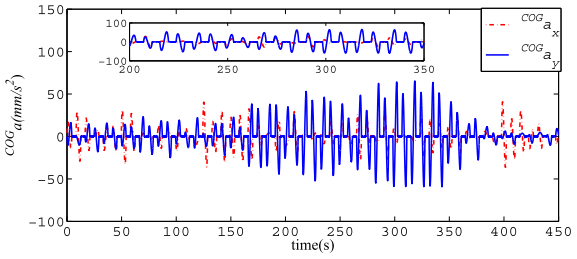

FIGURE 16. The velocity variation curve of COG with respect to $\{^{W}O\}$.

The changes of pitching angle (θ) and rolling angle (β) of body during the walking process of robot are respectively shown in Fig.17. It can be seen that the values of α and β are all varies in a small range. That demonstrated movement stability of body when quadruped robot use the gait planning method propose in this paper. Fig.18 shows the screen shots of quadruped robot walking on a single step and stair in simulation environment. It is proved that quadruped robot can walking on different types of rough terrain by using the static gait planning method proposed in this paper.

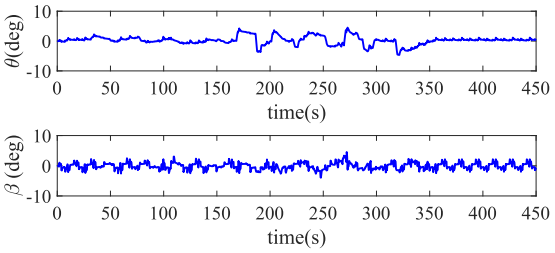

FIGURE 17. The attitude angle variation curve of the robot's body during the quadruped robot walking process.

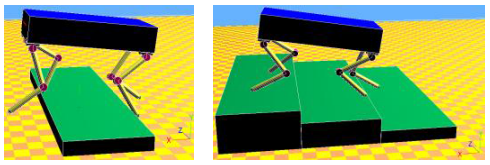

(a)Quadruped robot walking on single step. (b)Quadruped robot going up stair.

FIGURE 18. Screen shots of quadruped robot walking on different types of rough terrain in simulation environment.

VI. CONCLUSION

This paper presents a continuous static gait planning method, which lays a good theoretical foundation for improving the terrain adaptability of quadruped robot. By using the proposed method, quadruped robot can real-time estimate terrain complexity by using touchdown times of swing feet in real-time without any machine vision system. The body trajectory planning method based on quintic equation can effectively ensure motion continuity and stability of quadruped robot in its walking process. By using the given relationship between the terrain complexity estimation and the tunable parameter in body trajectory planning method, quadruped robot can generate its body trajectory according to the terrain complexity autonomously. The terrain adaptability and energy utilization rate of quadruped robot can be effectively improved in this way. The simulation experiment results showed that quadruped robot can walk through the terrain with different complexity by using the proposed gait planning method stably and efficiently.

The method proposed in this paper can be only used when quadruped robot walk on the terrains without forbidden areas. In the future work, the proposed gait planning method will be further improved to help quadruped robot travel over the terrains with forbidden areas.

REFERENCES

[1] Y. Li, B. Li, J. Ruan, and X. Rong, "Research of mammal bionic quadruped robots: A review," in *Proc. IEEE 5th Int. Conf. Robot., Automat. Mechatronics (RAM)*, Sep. 2011, pp. 166–171.

[2] R. B. Mcghee and A. Frank, "On the stability properties of quadruped creeping gaits," *Math. Biosci.*, vol. 3, no. 1, pp. 331–351, 1968.

[3] S. Ma, T. Tomiyama, and H. Wada, "Omnidirectional static walking of a quadruped robot," *IEEE Trans. Robot.*, vol. 21, no. 2, pp. 152–161, Apr. 2005.

[4] H. Hwang and Y. Youm, "Steady crawl gait generation algorithm for quadruped robots," *Adv. Robot.*, vol. 22, nos. 13–14, pp. 1539–1558, 2008.

[5] C. P. Santos and V. Matos, "Cpg modulation for navigation and omni-directional quadruped locomotion," *Robot. Auto. Syst.*, vol. 60, no. 6, pp. 912–927, 2012.
[6] X. Chen, K. Watanabe, K. Kiguchi, and K. Izumi, "Translational crawl and path tracking of a quadruped robot," *Adv. Robot.*, vol. 19, no. 12, pp. 569–584, 2002.
[7] V. G. Loc, I. M. Koo, D. T. Tran, S. Park, H. Moon, and H. R. Choi, "Improving traversability of quadruped walking robots using body movement in 3D rough terrains," *Robot. Auto. Syst.*, vol. 59, no. 12, pp. 1036–1048, 2011.
[8] P. Fankhauser, M. Bjelonic, C. D. Bellicoso, T. Miki, and M. Hutter, "Robust rough-terrain locomotion with a quadrupedal robot," in *Proc. IEEE Int. Conf. Robot. Autom. (ICRA)*, May 2018, pp. 5761–5768.
[9] S. Bazeille, V. Barasuol, M. Focchi, I. Havoutis, M. Frigerio, J. Buchli, C. Semini, and D. G. Caldwell, "Vision enhanced reactive locomotion control for trotting on rough terrain," in *Proc. IEEE Int. Conf. Technol. Practical Robot Appl.*, Apr. 2013, pp. 1–6.
[10] J. Z. Kolter, Y. Kim, and A. Y. Ng, "Stereo vision and terrain modeling for quadruped robots," in *Proc. IEEE Int. Conf. Robot. Autom.*, May 2009, pp. 1557–1564.
[11] M. Kalakrishnan, J. Buchli, P. Pastor, M. Mistry, and S. Schaal, "Fast, robust quadruped locomotion over challenging terrain," in *Proc. IEEE Int. Conf. Robot. Autom.*, May 2010, pp. 2665–2670.
[12] M. Kalakrishnan, J. Buchli, P. Pastor, M. Mistry, and S. Schaal, "Learning, planning, and control for quadruped locomotion over challenging Terrain," *Int. J. Robot. Res.*, vol. 30, no. 2, pp. 236–258, 2011.
[13] J. Zico Kolter and A. Y. Ng, "The stanford littledog: A learning and rapid replanning approach to quadruped locomotion," *Int. J. Robot. Res.*, vol. 30, no. 2, pp. 150–174, 2011.
[14] M. Zucker, N. Ratliff, M. Stolle, J. Chestnutt, J. A. Bagnell, C. G. Atkeson, and J. Kuffner, "Optimization and learning for rough terrain legged locomotion," *Int. J. Robot. Res.*, vol. 30, no. 2, pp. 175–191, 2011.
[15] J. Z. Kolter, M. P. Rodgers, and A. Y. Ng, "A control architecture for quadruped locomotion over rough terrain," in *Proc. IEEE Int. Conf. Robot. Automat.*, May 2008, pp. 811–818.
[16] P. Filitchkin and K. Byl, "Feature-based terrain classification for LittleDog," in *Proc. IEEE/RSJ Int. Conf. Intell. Robots Syst.*, Oct. 2012, pp. 1387–1392.
[17] I. Havoutis, J. Ortiz, S. Bazeille, V. Barasuol, C. Semini, and D. G. Caldwell, "Onboard perception-based trotting and crawling with the hydraulic quadruped robot (HyQ)," in *Proc. IEEE/RSJ Int. Conf. Intell. Robots Syst.*, Nov. 2013, pp. 6052–6057.
[18] A. W. Winkler, C. Mastalli, I. Havoutis, M. Focchi, D. G. Caldwell, and C. Semini, "Planning and execution of dynamic whole-body locomotion for a hydraulic quadruped on challenging terrain," in *Proc. IEEE Int. Conf. Robot. Autom.*, May 2015, pp. 5148–5154.
[19] A. Chilian and H. Hirschmüller, "Stereo camera based navigation of mobile robots on rough terrain," in *Proc. IEEE/RSJ Int. Conf. Intell. Robots Syst.*, Oct. 2009, pp. 4571–4576.
[20] X. Shao, Y. Yang, and W. Wang, "Obstacle crossing with stereo vision for a quadruped robot," in *Proc. IEEE Int. Conf. Mechatronics Automat.*, Aug. 2012, pp. 1738–1743.
[21] M. Wermelinger, P. Fankhauser, R. Diethelm, P. Krüsi, R. Siegwart, and M. Hutter, "Navigation planning for legged robots in challenging terrain," in *Proc. IEEE/RSJ Int. Conf. Intell. Robots Syst. (IROS)*, Oct. 2016, pp. 1184–1189.
[22] P. G. De Santos, E. Garcia, and J. Estremera, *Quadrupedal Locomotion: An Introduction to the Control of Four-Legged Robots*. Berlin, Germany: Springer, 2007.

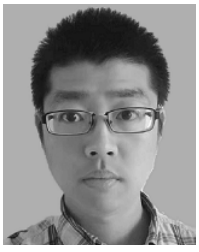

SHUAISHUAI ZHANG received the bachelor's degree from the Shandong University of Technology, China, in 2009, and the master's and Ph.D. degrees from Shandong University, China, in 2012 and 2016, respectively. He is currently a Lecturer with the Department of Electrical Information, Shandong University of Science and Technology, China. His research interests include robotics technology and intelligent systems.

MING LIU received the bachelor's and master's degrees from the Shandong University of Science and Technology, China, in 1995 and 1998, respectively. He is currently pursuing the Ph.D. degree with the School of Control Science and Engineering, Shandong University, China. He is also an Associate Professor and the Vice Dean with the Department of Electrical Information, Shandong University of Science and Technology. His research interests include robotics, intelligent control, and intelligent vehicles.

YANFANG YIN received the bachelor's and master's degrees from the Shandong University of Science and Technology, China, in 1999 and 2002, respectively, where she is currently pursuing the Ph.D. degree. She is also a Lecturer with the Department of Electrical Information, Shandong University of Science and Technology. Her research interest includes machine learning.

XUEWEN RONG received the bachelor's and master's degrees from the Shandong University of Science and Technology, China, in 1996 and 1999, respectively. He is currently pursuing the Ph.D. degree with the School of Control Science and Engineering, Shandong University, China. He is also a Senior Engineer with Shandong University. His research interests include robotics, mechatronics, and hydraulic servo driving technology.

YIBIN LI received the bachelor's degree from Tianjin University, China, in 1982, the master's degree from the Shandong University of Science and Technology, China, in 1988, and the Ph.D. degree from Tianjin University, in 2006. He is currently a Professor and the Associate Dean with the School of Control Science and Engineering, Shandong University, China. His research interests include robotics, mechatronics, intelligent control, and intelligent vehicles.

ZISEN HUA was born in 1988. He received the B.S. and M.S. degrees from Shandong Jianzhu University, China, in 2011 and 2014, respectively. He is currently pursuing the Ph.D. degree with Shandong University, China. His research interests include mechanical structure optimization and analysis, hydraulic servo transmission, and control systems.